CHINESE JOURNAL OF PHYSICS VOL. 30, NO. 6 DECEMBER 1992

Orientation-dependent X-ray Absorption Fine Structure (XAFS) of the Bi-St=Ca-Cu-0 System

C. H. Chou, W. F. Pong[1], J. B. Shi[2], H. C. Ku[3], and I. N. Lin[4]

Department of Physics, Nutionul Tuiwun University, Taipei, Tuiwun 107, R.O.C.

[2]*Department of Physics, Tumkung University, Tamsui, Tuiwun 251, R.O.C.*

[1]*Institute of Electronics, Nutionul Chiuo Tung University, Hsinchrc, Tuiwun 300, R.O.C.*

[3]*Department of Physics, Nutionul Tsing Huu University, Hsinchu, Tuiwun 300, R.O.C.*

[4]*Materials Science Center, Nutionul Tsing Hua University, Hsinchu, Tuiwun 300, R.O.C.*

(Received June 1, 1992; revised manuscript received June 27, 1992)

Using the transmission and fluorescence modes at the National Synchrotron Light Source (NSLS) X-23A2 beam line, we have measured polarized XAFS spectra of the Bi, Pb L_3-edges and the Cu K-edge for the $(Bi_{1.85}Pb_{0.15})Ca_{2.2}Sr_{1.8}Cu_3O_{10+\delta}$ sample and unpolarized XAFS spectra of the Bi, Pb L_3-edges and the Cu K-edge for $Bi_2Ca_{1.2}Sr_{1.8}Cu_2O_{8+\delta}$, $Pb_{0.2}Bi_{1.9}Sr_{1.9}Cu_1O_{6+\delta}$ and $(Pb_xBi_{2-x})Sr_2Ca_2Cu_3O_y$ (x = 0, 0.2, 0.4) samples. All XAFS spectra were measured at room temperature. The incommensurate modulations in the Bi-0 layers are discussed in terms of the XAFS technique. The XAFS spectra of Bi L_3-edge do not vary substantially for different sample orientation with respect to the X-ray polarization vector E. There is evidence for the existence within the Bi-Sr-Ca-Cu-0 system of Bi atoms having the oxidation number exceeding 3. Pb ions predominantly substitute for Bi ions in the Bi-Sr-Ca-Cu-0 system because there is no significant difference between the XANES spectra of the Pb and Bi L_3-edges, respectively. The oxidation numbers of substituted Pb in Bi-Sr-Ca-Cu-0 system differ much from those of Pb in PbO_2 in which the oxidation number of all Pb atoms is 4. In agreement with other investigators, our results on the polarized XANES spectra of the Cu K-edge indicate that a satellite about 7 eV above the main K-XANES peak in both polarizations is a multielectron excitation to the final-state configuration $\underline{1s}3d^9\varepsilon p^1$, and that a shoulder on the rising absorption edge, present for many Cu compounds and generally assigned to a shake-clown multielectron excitation, is a transition to a final state of the Cu compounds. We have also deduced that the structure of the Cu-0 planes in the Bi-Sr-Ca-Cu-0 samples is ordered.

I. INTRODUCTION

Following the discoveries of the oxide superconductors La-Sr-Ca-O[1] and Ba-Y-Cu-0,[2] further superconductors Bi-Sr-Ca-Cu-0 (BSCCO) containing no rare-earth elements and with $T_c \sim 110$ K and $\sim$ SO K were reported by Maeda et al.;[3] the latter phases were rapidly identified

as $Bi_2Sr_2Ca_2Cu_3O_{10+\delta}$ with T_c (max) $\approx$ 110 K and $Bi_2Sr_2CaCu_2O_{8+\delta}$ with T_c (max) $\approx$ 95 K. Including $Bi_2Sr_2CuO_{6+\delta}$ with T_c (max) $\approx$ 32 K, previously discovered by Michel et al.[4] and Akimitsu et al.,' a series of compounds was formulated and expressed as $Bi_2Sr_2Ca_{n-1}Cu_nO_{2n+4+\delta}$ with n = 1, 2, 3 (n is the number of consecutive Cu-0 layers). The members of this series are commonly designated 2201, 2212 and 2223 respectively according to the ratio of metallic cations in the chemical compositions.

Under normal conditions of preparation, the 2212 type appears to be the most stable and commonly predominates even when the initial composition is intended to favor 2223. Great effort has been expended to prepare the 2223 phase in pure form. There are several procedures[6] that have been found to increase the volume fraction of the 2223 phase. The key of these procedures is the addition of Pb to the composition of Bi-Sr-Ca-Cu-O.[7] The influence of Pb substitution on the Bi-Sr-Ca-Cu-0 system is related closely to the location and oxidation number of the substituted Pb. Lead ions substitute mainly for bismuth ions in the Bi-Sr-Ca-Cu-0 system; this 'deduction, which is still debated,[8,9] originates from the result of local chemical electron microanalysis,[10] but relies on few experimental facts.[11,12] In contrast with this evidence, from a neutron-diffraction study on powders the location of most Pb ions was assigned to calcium sites.[13] The conclusions about the oxidation numbers of the substituted Pb are controversial.[14] The extra oxygen is commonly observed with the appearance of incommensurate modulation (*vide infra*) in the Bi-0 layers and creates holes that are considered possibly responsible for superconductivity. The electronic properties, such as metallic nature, of the Bi-0 layers seemingly plays an essential role in superconductivity." However, because the structures of the Bi-0 layers are extremely complicated, the related properties of the Bi-0 layers have not yet been definitively elucidated. It is still desirable and proves challenging to lift the uncertainty about the issues mentioned above.

The X-ray absorption fine structure (XAFS)[16] is conventionally distinguished into two regions: X-ray absorption near-edge spectrum (XANES) and extended X-ray absorption fine structure (EXAFS). XANES spectroscopy gives unique information on the local electronic structure at various atomic sites in these systems formed by diverse atoms with a complex structure. Polarized XANES spectroscopy provides information about the orbital angular momentum of the unoccupied states according to the selection rules. Therefore the application of (polarized) XANES spectroscopy to high-T, superconductors is of interest. The photoelectron in the final state for $\mathbf{E} \perp \mathbf{C}$ polarization probes mainly the atomic distribution in the Cu-0 planes, whereas for $\mathbf{E} \parallel \mathbf{C}$ polarization it probes the atomic distribution on adjacent SrO and Ca planes. (E is the X-ray polarization.) Hence, polarized spectra are of key importance for a correct interpretation of XANES spectra of anisotropic crystals. In the EXAFS region, the strong anisotropy of the unbound final state of photoelectron for the polarized absorption spectrum of the K-edge allows us to employ spectra to probe orientation-dependently the local structure with intrinsic anisotropy around the absorbing atom.

Great efforts have been expended to separate and to distinguish the features of XANES of the Cu K-edge of superconductors. After reliably interpreting the features of XANES of the Cu K-edge, which relates to peculiar aspects of the local electronic structure around the Cu atom within Cu-0 planes, one can utilize the versatile XAFS techniques to obtain desired experimental data which are of benefit to probe the electronic properties of the Cu-0 planes of the prepared sample under consideration. Because various theories to explain the pairing mechanism depend heavily on the electronic properties, the understanding of the electronic properties of high-T, superconductors is of value to decide which theories are more likely to be correct, and would stimulate speculation about the possible mechanism of superconductivity.

By employing the XAFS techniques and by considering the results of auxiliary experiments on the samples, we have succeeded in clarifying some ambiguous statements concerning the properties of the Bi-0 layers and the influence of Pb substitution. Taking into account the theoretical and experimental data reported from recent studies, we have more conclusively interpreted the features of XANES spectra of the Cu K-edge of the Bi-Sr-Ca-Cu-0 system and provided XAFS evidence which is desirable to confirm the current conclusions about features of the Cu K-edge. In addition, some properties of the Cu-0 plane are also considered.

II. EXPERIMENTAL PROCEDURE

II-l. Sample preparation and characterization

We synthesized two sets of superconducting samples using a solid-state reaction method. High-purity powders of Bi_2O_3, Pb_3O_4, $CaCO_3$, $SrCO_3$, La_2O_3 and CuO were used with the ratios (Bi+Pb):Sr:Cu = $(1.9+0.2)$:1.9:1 for the (2201) sample, Bi:(Ca+Sr):Cu = 2:$(1.2+1.8)$:2 for the (2212) sample and $(Bi+Pb)$:(Ca + Sr):Cu = $(1.85+0.15)$:$(2.2+1.8)$:3 for the (2223) sample. Well-mixed powders were calcined at 800 °C in air for 1 day with several intermediate regrinding. These powders were then pressed into pellets and sintered at 850 °C in air up to 1 day and then either liquid nitrogen quenched or quenched in air (both were performed in this study) for the (2201) samples; at 850 °C up to **15** hours and then liquid nitrogen quenched for the (2212) sample; and at 859 °C up to 3 days and then furnace cooled for the (2223) sample. Sintering conditions were determined from differential thermal analysis (DTA) data by means of an ULVAC model 7000 symmetrical thermomicrobalance. Powder X-ray diffraction (XRD) data for random oriented powders and epoxy-embedded aligned powders were obtained using a Riguku D/MAX B diffractometer to identify the phases of the samples and to analyze the degree of c-axis alignment. Superconducting data of these samples were obtained by using a Quantum Design MPMS SQUID magnetometer with 2 K to 300 K and applied magnetic field up to ± 5.5 T. For zero-field-cooled measurements, the "magnetic reset" option was used to quench the superconducting magnet and reduce the residual or remnant field to less than 1 G. For the double Cu-O layers (n = 2) system with the $Bi_2Sr_2Ca_1Cu_2O_{8+\delta}$-type 2212 structure, the

$Bi_2Sr_{1.8}Ca_{1.2}Cu_2O_{8+\delta}$ compound was chosen for the location of the composition inside the single-phase line $Bi_2Sr_{2-x}Ca_{1+x}Cu_2O_{8+\delta}$ ($0 \leq x \leq 0.75$).[17] For the three Cu-0 layers ($n = 3$) system with the $Bi_2Sr_2Ca_2Cu_3O_{10}$ +&type 2223 structure, the $(Bi_{1.85}Pb_{0.15})Sr_{1.8}Ca_{2.2}Cu_3O_{10+\delta}$ compound was chosen to ensure the single-phase property of the 2223 structure.[18] For the single Cu-0 layers ($n = 1$) system with the $Bi_2Sr_2Cu_1O_{6+\delta}$-type 2201 structures, the $(Bi_{1.9}Pb_{0.2})Sr_{1.9}Cu_1O_{6+\delta}$ compounds quenched in air and in liquid N_2 were chosen to ensure the single-phase property of the 2201 structure. The measured data for the 2223 and 2212 samples were discussed in Ref. 19 in detail. The temperature dependence of electrical resistivities, measured by means of the four-probe method, shown in Fig. 1, reveals that $T_c = 13$ K for the 2201 samples quenched in liquid N_2 and that the sample quenched in air presents nonsuperconductivity. Fig. 1 also shows the magnetic susceptibility of the 2201 sample (T, = 13 K). All lines of the XRD pattern for the random oriented powders of the 2201 sample with $T_c = 13$ K, shown in Fig. 2, can be indexed with 2201 structure. This indicates that excellent single-phase samples with single Cu-0 layer structure were prepared. The single-phase samples extracted from $(Bi_{1.85}Pb_{0.15})Sr_{1.8}Ca_{2.2}Cu_3O_{10+\delta}$, $Bi_2Sr_{1.8}Ca_{1.2}Cu_2O_{8+\delta}$ and $(Bi_{1.9}Pb_{0.2})Sr_{1.9}Cu_1O_{6+\delta}$ compounds are denoted the 2223 sample, the 2212 sample and two 2201 samples (one with $T_c = 13$ K, the other nonsuperconductive) respectively in what follows.

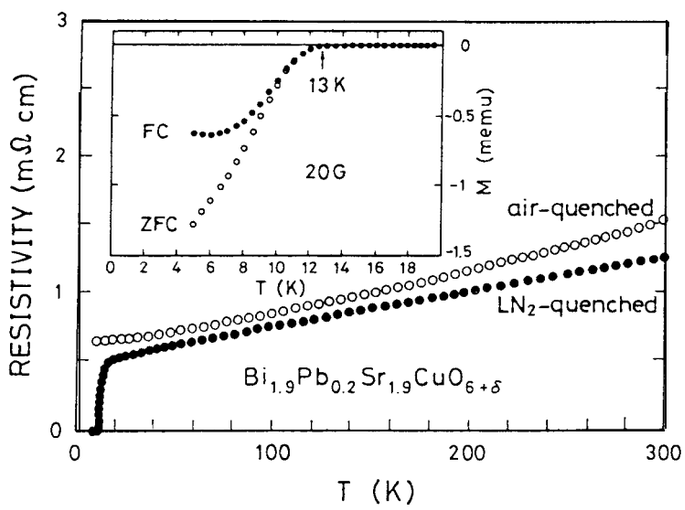

FIG. 1. Temperature dependence of electrical resistivities for the 2201 sample quenched in air and for the 2201 sample quenched in liquid N_2. The inset shows temperature dependence of magnetization M(T) for the 2201 sample quenched in liquid N_2, field cooled (FC) and zero-field cooled (ZFC) with applied field II = 20 G.

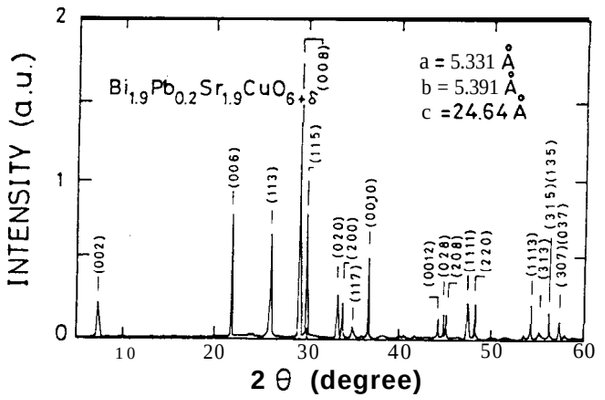

FIG. 2. X-ray-diffraction pattern for the powder sample $Bi_{1.9}Pb_{0.2}Sr_{1.9}CuO_{6+\delta}$ with $T_c = 13K$.

We prepared superconducting compounds in another series having nominal composition $(Pb_xBi_{2-x})Sr_2Ca_2Cu_3O_y$ with x = 0, 0.2, 0.4 (hereafter described as Pb-BSCCO), using PbO, Bi_2O_3, $SrCO_3$, $CaCO_3$ and CuO powders of at least 99.9 % purity. The mixed powders of appropriate proportions were calcined in air at 800 °C for 4 hours, ground, calcined again in air at 820 °C for further 4 hours, and then reground. The reground samples were pressed into pellets and sintered in air at 860 °C for 192 hours. Another sample with x = 0 were prepared by the same process, except that the duration of sintering was 96 hours. (We refer below to this sample by specifying its sintering duration.) We determined the superconducting transition temperature (T_c) of each sintered sample from the temperature dependence of the ac susceptibility (χ_{ac}), using a Sumitomo Model SCR 204 T measuring system at 1 KHZ. The crystal structure and phase constituents of the corresponding samples were determined by means of the XRD technique (Rigaku, Cu Ka). The experimental data reveal that almost only the 2212 phase is observed for the Pb-BSCCO samples (x = 0.0, 0.2) and, in contrast, the Pb-BSCCO sample (x = 0.4) are predominantly the 2223 phase, with a small proportion of 2212 phase coexisting. Detailed experimental procedures and characterization of the Pb-BSCCO (x = 0.0, 0.2, 0.4) samples were given in Ref. 20.

11-2. X-ray absorption measurements

X-ray absorption measurements were performed on beam line X-23A2 of the National Synchrotron light Source (NSLS) with a Si(220) double-crystal monochromator and ion-chamber detectors. Mirror was used to remove the higher order harmonics. During this run, the NSLS was operated at an energy 2.528 GeV and an electron current 234-195 mA. The photon energy for each measurement (Cu K-edge, Pb L_3-edge, and Bi L_3-edge) was simultaneously

calibrated by means of Cu foil, PbO and Bi_2O_3, which were placed after the corresponding samples. The data were measured in the fluorescence or transmission mode. The energy resolution $\Delta E/E$ was approximately equal to 10^{-4} for each measurement. The XAFS samples were ground into fine powders ($\sim$ 400 mesh), and then spread uniformly onto adhesive cellulose tape which was then folded in order to provide the desired thickness. All spectra were measured at room temperature.

To perform anisotropic X-ray-absorption measurements, we used the magnetic orientation technique of Farrel et al.[21] A sintered single-phase superconducting pellet (the 2223 sample) was ground to powder with average microcrystalline grain size l-10 μm, and mixed with SPAR 5-minute epoxy hardener in a quartz holder of diameter 8 mm in proportions appropriate for XAFS measurements (powder: epoxy ratio $\approx$2:1). The mixture was spread onto an adhesive cellulose tape that was aligned in a 9.4-tesla superconducting magnet (Bruker, Germany) at room temperature; the alignment was checked by X-ray diffraction measurements. The (001) peaks of the XRD data are predominant in the aligned sample in which the degree of alignment is better than 90 %, and confirm the anticipated c-axis orientation along the applied field at room temperature.

III. DATA ANALYSIS AND DISCUSSION

III-1. Bi L_3-edge

Because there are at least four times as many Bi atom as Pb atoms in the Pb-modified superconducting samples in our work, there is no significant contribution from XAFS of the Pb L_3-edge which extends past the Bi L_3-edge although the two edges are separated by only AE = 380 eV. Neglecting the fine structure of the absorption spectra of the Pb L_3-edge in the range above the Bi L_3-edge and treating those as the background, we reliably obtain XAFS spectra of the Bi L_3-edge simply by removing the background.

We define the EXAFS function X(k) as[22]

$$\chi(k) = \frac{\mu(E) - \mu_0(E)}{\mu_0(E)} \tag{1}$$

in which μ is the absorption coefficient, μ_0 is the structureless absorption coefficient of the isolated atom in question, and k is the wave vector of the ejected photoelectron. The X-ray cnergy E is converted into the wave vector k by means of the equation

$$k = [2m_e(E - E_0)/\hbar^2]^{\frac{1}{2}}. \tag{2}$$

Here E_0 is the so-called threshold energy, m_e is the mass of clcctron, and cnergy and wave vector are conventionally expressed in the units eV and $Å^{-1}$ respectively. As we mentioned previously,[20] the existence of the modulation structures is monitored by means of the EXAFS tech-

nique. Here, we did similar measurements of unpolarized EXAFS spectra for Pb-BSCCO samples (x = 0, 96 h and x = 0, 192 h) and for the 2223, 2212 and 2201 (T, = 13 K, non-superconductive) samples. The magnitudes of the Fourier transforms of the k%(k) data sets of Bi_2O_3, the Pb-BSCCO samples (x = 0, 96 h and x = 0, 192 h) and of the 2223, 2212 and 2201 (T, = 13 K, non-superconductive) samples, are collectively depicted in Fig. 3(a) and (b). The magnitude of each Fourier transform of k%(k) reveals peaks corresponding to the shells of neighbours around the absorbing Bi atoms. Curve (a_1) in Fig. 3(a) refers to the magnitude of the Fourier transform of k%(k) of Bi_2O_3. Because there are oxygen atoms in two nonequivalent types of coordination[23] around the bismuth atoms within Bi_2O_3 and because the Bi-0 coordination in the structure is classified in two distinct ranges 2.08-2.29 Å and 2.48-2.80 Å, the first peak corresponding to the nearest oxygen atoms is broad; the peak located near 3.5 Å indicates the other Bi atoms around the Bi absorbing atoms. Curves $(b_1), (c_1)$ in Fig. 3(a), and curves (d_1), $(e_1), (f_1)$ and (g_1) in Fig. 3(b) show the magnitudes of the Fourier transforms of the $k^2\chi(k)$ data of the BSCCO sample (x = 0, 96 h), the BSCCO sample (x = 0,192 h), the 2201 samples without superconductivity and with T_c = 13 K, and the 2212 and 2223 samples, respectively. The first peak in each plot corresponds obviously to the nearest oxygen atoms in the Bi-0 layers. No appreciable overlap of different atomic species occurs before the second peak which contains Bi-

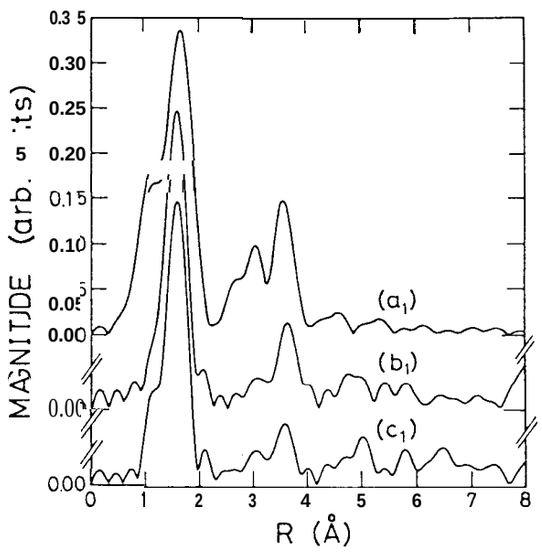

FIG. 3(a). Magnitudes of Fourier transforms of the $k^2\chi(k)$ data (L_3-edge absorption of Hi) of (at) Bi_2O_3, (b_1) the BSCCO sample (x = 0.0, 96 hrs), and (cl) the BSCCO sample (x = 0.0, 192 hrs), obtained by transforming over the k-ranges 2.13-11.23, 2.23-11.73, and 2.23–11.58 $Å^{-1}$ respectively, and by choosing E_0 at the half-height point of the absorption coefficient μ.

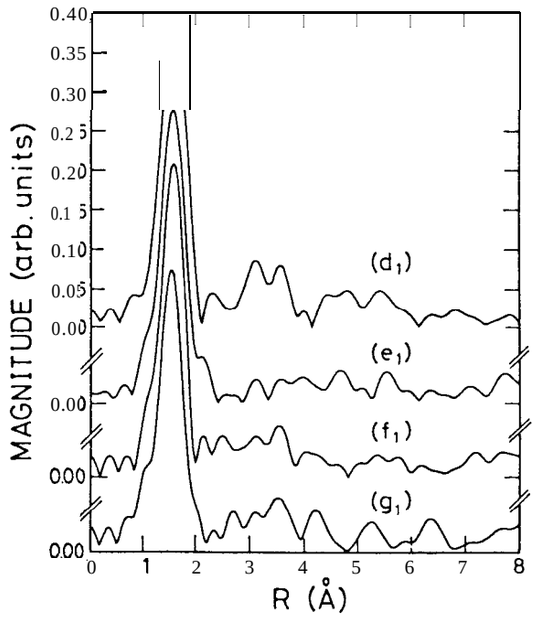

FIG. 3(b). Magnitudes of Fourier transforms of the $k^2\chi(k)$ data (L_3-edge absorption of Bi) of the 2201 samples (d_1) non-superconductive and (e_1) with T_c = 13 K, (f_1) the 2212 sample, and (g_1) the 2223 sample, obtained by transforming over the k ranges 2.23-11.13, 2.23-10.98, 2.23-11.03 and 2.23–11.03 $Å^{-1}$ respectively, and by choosing E_0 at the half-height point of the absorption coefficient/c.

Sr(Ca) and Bi-Bi components and would be expected to be located near 3.5 Å in each plot. Of particular interest is that the second peak shows an exceptionally small amplitude. The disappearance of the second peak in the Fourier transform of the $k^2\chi(k)$ data of each sample implies that there occurs an anomalous static disorder of the distances between the absorbing Bi atoms and the nearest neighboring Bi, Ca, Sr atoms. The incommensurate modulations within the Bi-0 layers in the Bi-Sr-Ca-Cu-0 family have been investigated by means of X-ray single-crystal diffraction, X-ray and neutron diffraction of powders and transmission electron microscopy (TEM).[24,25] Each Bi-0 layer contains occupational and positional fluctuation of Bi sites which results in "Bi-concentrated bands" and "Bi-deficient bands" and an accompanying displacement of atoms in the Bi-0, Sr-0, Cu-0 and Ca layers from their average position. Schncck et al.[26] and Wen et al.[27] reported that the basic structure of the incommensurate modulation within the lead-free compounds is preserved in the Pb-modified Bi-Sr-Ca-Ca-0 system. The reduction of the second peak in the Fourier transform of the $\chi(k)$ data of each sample is caused by periodic displacements of the corresponding metallic atoms from their average position in the modulated structure and is the signature of the occurrence of the modulation structures in all samples. For

the Bi L_3-edge of the BSCCO sample (x = 0, 96 h) the relative height of the second peak of the magnitude of the Fourier transform of the X(k) data measured in our previous work[20] is greater than that of the second peak of the Fourier transform of the $\chi(k)$ data measured recently for the Bi L_3-edge of the same sample. This result indicates the progressive appearance of the modulation structure in the BSCCO sample (x = 0, 96 h) and reflects that the modulation structures seem more stable. Fig. 4. illustrates the total phase of the Fourier-filtered X(k) data from the first peak located in the range of R 0.8-2.01 Å in each plot, depicted in Fig. 3(a), (b). According to the beat-node method, the minimum point (beat node) of the amplitude of the Fourier-filtered X(k) data, and the associated kink in the total phase, reveal the difference AR of the bond distances of a coordinate shell from the equation $k_b = (\pi/2\Delta R)$. Because of the variation of the bond distances of the nearest oxygen atoms around the Bi atom in Bi_2O_3, the beat nodes, indicated by arrow mark, appear in the total phase. Because no salient beat node appears in the total phases of the Fourier-filtered $\chi(k)$ data from the first peak corresponding to the nearest oxygen atoms around the Bi atom in each BS(C)CO sample within the k range with $k_{max} \approx 10$ Å^{-1}, we suggest that most nearest neighbor oxygen atoms around the Bi atoms within Bi-0 layers are located at almost the same distance (AR $\leq \pi/2k_{max} \approx 0.16$ Å) from the Bi atom.

The XANES spectrum of the Cu L_3-edge for the Bi-Sr-Ca-G-0 system has enabled the successful determination of the occupancy of the $d_{x^2-y^2}$ and $d_{3z^2-r^2}$ orbital? of Cu. The orien-

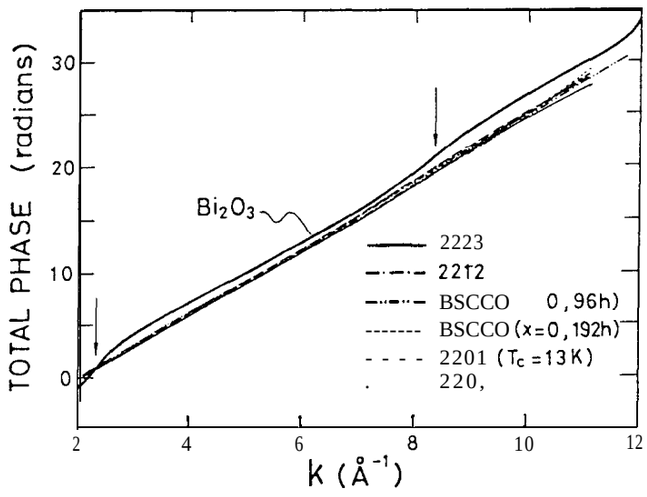

FIG. 4. Total phases of the inverse transforms (the Fourier-filtered $\chi(k)$ spectra) from the first peaks, located in the K-range 0.8–2.01 Å, of the Fourier transforms of the XAFS spectra depicted in Fig. 3 (a) (b)..

tation dependence of XANES spectra of the Cu L_3-edge depends on the other 3d orbitals being occupied. In the EXAFS region in which the final states of photoelectron ejected by a monochromatic X-ray are unbound and empty completely, or in the case of XANES of the material in which the orbitals of d symmetry are totally unoccupied or totally occupied, it becomes more difficult and complicated to employ XAFS data of the L_3 edge to investigate the geometry of the local structure and electronic states around the absorbing atoms. The general EXAFS expression for L_2 and L_3 edges is[29]

$$\begin{aligned}\chi(k) = \sum_i \sum_j A_i^*(k)\Big\{ & \frac{1}{2}(1+3\cos^2\alpha_{ij})M_{21}^2 \sin[2kR_i+\phi_2^i] \\ & +(1-3\cos^2\alpha_{ij})M_{01}M_{21}\sin[2kR_i+\phi_{02}^i] \\ & +\frac{1}{2}M_{01}^2\sin[2kR_i+\phi_0^i]\Big\}\left(M_{21}^2+\frac{1}{2}M_{01}^2\right)^{-1}\end{aligned} \tag{3}$$

The summation extends over all j atoms in the i'th neighbor shell at a distance R_i and with an *effective* scattering amplitude A_i^*. α_{ij} is the angle between the electric field vector **E** of the X-ray and the internuclear axis from the absorbing atom to the backscattering atom j in the i'th shell. M_{01} and M_{21} are radial dipole matrix elements for transitions from $l = 1$ initial to $l = 0$ and $l = 2$ final states, respectively. The scattering phase shifts $\phi(k)$ are those experienced by the photoelectron from the absorbing (6) and backscattering (t) atoms:

$$\phi_\ell^i(k) = 2\delta_\ell(k) + \tau_i(k), \tag{4}$$

$$\phi_{02}^i(k) = \delta_0(k) + \delta_2(k) + \tau_i(k). \tag{5}$$

The influence of atoms beyond the first oxygen shell on the polarized XAFS spectrum of the Bi L_3-edge is reduced due to the peculiar structure of the incommensurate modulations in the Bi-0 layer; the local coordination geometry of the nearest oxygen atoms around the Bi atom has isotropic symmetry despite the strong two-dimensional character of the structure of the Bi-Sr-Ca-Ca-0 system. For these two reasons, neither polarized XANES spectra of the Bi L_3-edge, which is caused by the transition to the completely empty states with d symmetry, nor the polarized EXAFS spectra of the Bi L_3-edge, which would be expected to reflect no orientation dependence according to the formula derived by Stöhr et al.,[29] exhibit the orientation dependence. We have measured the $\mathbf{E}\|\mathbf{C}, \mathbf{E}\perp\mathbf{C}$ polarized and unpolarized XAFS spectra of the Bi L_3-edge of the 2223 sample. The experimental XANES spectra reveal no prominent difference from each other. The magnitudes of the Fourier transforms of the polarized ($\mathbf{E}\|\mathbf{C}, \mathbf{E}\perp\mathbf{C}$) and unpolarized EXAFS spectra of the Bi L_3-edge for the 2223 sample are also similar. Similarly, in the case of the Pb L_3-edge, the orientation dependence of the XAFS spectra of the polarized 2223 sample is also not detectable. Employing polarized XAFS spectra of the Bi L_3-edge (or

of the Pb L_3-edge) to probe the orientation dependence of the electronic and structural features around the Bi atom (or the Pb atom) within the Bi-Sr-Ca-Ca-0 system is futile.

Because the XANES spectrum of the Bi L_3-edge for each of the 2223, 2212, 2201 (T, = 13 K and non-superconductive) samples, and the Pb-BSCCO samples with x = 0.2, 0.0 strongly resemble the XANES spectra of the others, it is difficult to monitor the possible minute variations of the average oxidation number of Bi between these samples based on XANES data. It is beneficial to examine the derivative of the XANES spectra of the samples shown in Fig. 5. Based on band-structure calculations, we expect the low-lying states to consist of Bi(6s) and O(2p) states in the samples. For the Bi L_3-edge the dipole selection rules allow direct transitions

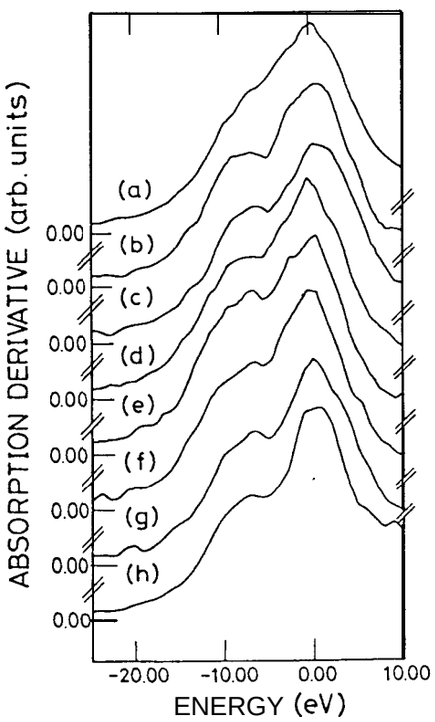

FIG. 5. Derivatives of the normalized X-ray-absorption near-edge structures measured at the Bi L_3-edge of (a) Bi_2O_3, (b) the 2223 sample, (c) the 2212 sample, the 2201 samples with (d) T_c = 13 K and (e) non-superconductive, and the Pb-BSCCO samples with (f) x = 0.2 and (g) x = 0.0. The zero of the energy scale is at the vicinity of the raising edge of each spectrum of the Bi L_3-edge. For comparison, the derivative of the normalized X-ray-absorption near-edge structure measured at the Pb L_3-edge for (h) Pb_3O_4 is illustrated simultaneously. The energy zero in the case of the Pb L_3-edge refers to 13035 eV.

to empty Bi(6s) states; the occurrence of a low-lying bump corresponding to the transition to the Bi(6s) orbitals thus indicates the presence of empty Bi(6s) states and that the oxidation number of Bi in the compound exceeds 3. Reports by Salem-Sugui et al. and Heald et al.[30] support this interpretation. Because for Bi^{3+}, like the Bi cation within Bi_2O_3, these states are completely filled, the low-lying bump corresponding to the transition to Bi(6s) states is suppressed (curve (a)). The consistent existence of the bump located at about -6 eV, easily observed in each derivative of XANES spectra of the samples shown in Fig. 5 (peaks located at about -7 eV in curves (b)-(g)), reveals that within the Bi-Sr-(Ca)-Cu-0 system there are some Bi cations with oxidation number exceeding 3. Similarly, because in Pb_3O_4 there are Pb^{2+} and Pb^{4+} (Pb^{2+} cations in the majority),[31] the low-lying bump relating to the transition to empty Pb(6s) state is observed. The similarity of the derivative of the low-energy region of XANES spectrum of the Pb L_3-edge of Pb_3O_4 and the derivatives of the low-energy region of the XANES spectra of the Bi La-edge of the samples (cf. curve (h) and curves (b)-(g)) confirms that there is a proportion of Bi with oxidation number exceeding 3.

III-2. Pb **L_3-edge**

Examining the entire absorption spectra within the XANES range of the Pb-modified samples and of the lead-oxide compounds, we are able to find that the XANES spectra of the Pb L_3-edge of PbO and PbO_2 differ from those of the Pb L_3-edge of the samples; for this reason, the proportions of PbO and PbO_2 in each sample must be extremely small.

Figure 6(a) presents the XANES spectra of the Bi L_3-edge of the 2223, 2201 (T, = 13 K, non-superconductive) and the Pb-BSCCO (x = 0.2, 0.4) samples and those of the Pb L_3-edge of the same Pb-modified samples. Because there is no substantial change of XANES between the Pb and Bi L_3-edges for each sample, following the interpretation due to Boyce et al.[32] of superconductive $BaBi_{0.25}Pb_{1.75}O_y$, we suggest that most lead atoms in the additional lead-oxide compounds are situated in Bi-0 layers substituting for a portion of the Bi atoms. The conclusion is confirmed by the reproducible similarity of the first derivative of the high-energy region of the XANES spectra, which are sensitive to the local structure, of the Bi and Pb L_3-edges of each of the 2223, 2201 (T, = 13 K, non-superconductive) samples and the Pb-BSCCO (x = 0.2, 0.4) samples (shown in Fig. 6(b)). Despite the similarity of the experimental spectra of the Pb L_3-edge of Pb_3O_4 and of the Pb-modified samples, we eliminated the co-existence of the Pb_3O_4 phase in the samples by means of the XRD data of them. Therefore, the XAFS data without supplementary data from auxiliary measurements provide just the necessary evidence, but not sufficient evidence, of Pb substitution for Bi in the Bi-Sr-(Ca)-Cu-0 samples.

Figure 7 shows the low-energy region of the XANES-spectra, which is particularly sensitive to the electronic structure, of the Pb L_3-edge of the 2223, 2201 (T, = 13 K, non-superconductive) and Pb-BSCCO (x = 0.2, 0.4) samples; for each sample, the XANES spectra of PbO,

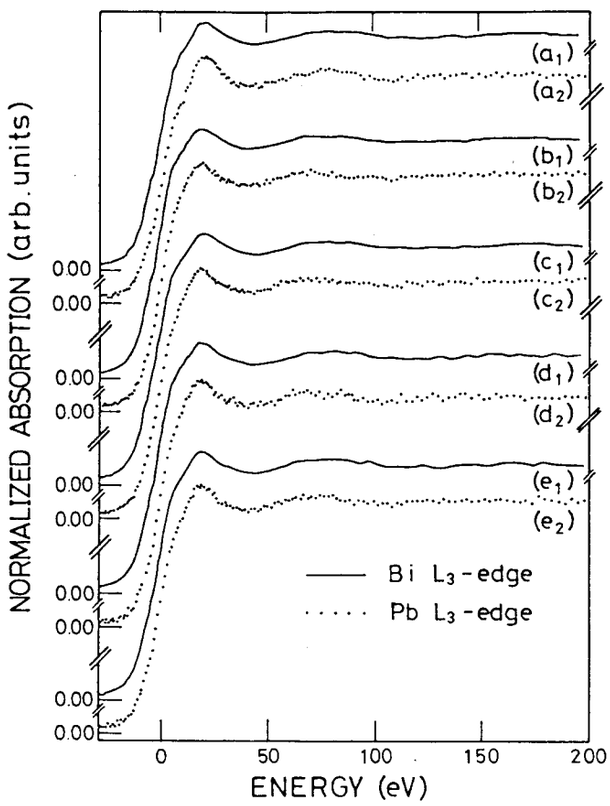

FIG. 6(a). The Bi L_3-edge absorption near-edge spectra for the 2223 sample (a_1), the 2201 samples with T_c = 13 K (b_1) and non-superconductive (c_1), the Pb-BSCCO sample (x = 0.2) (d_1), and the Pb-BSCCO sample (x = 0.4) (e_1); the energy zero in these spectra refers to 13422 eV. For comparison, the Pb L_3-edge absorption near-edge spectra of the 2223 sample (a_2), the 2201 samples with T_c = 13 K (b_2) and non-superconductive (c_2), the Pb-BSCCO sample (x = 0.2) (d_2), and the Pb-BSCCO sample (x = 0.4) (e_2); here the energy zero refers to 13035 eV. The vertical axis for each curve is normalized to give the same step height in arbitrary units.

Pb_3O_4, PbO_2 are superimposed simultaneously for comparison. Because the oxidation number of all Pb in PbO_2 is 4, so that the Pb(6s) orbitals are unoccupied, the low-lying bump corresponding to the transition to the Pb(6s) states, located at about -6 eV, is clearly observed in the XANES spectrum of Pb L_3-edge for PbO_2. This bump should also be observed in the XANES measurement of the compounds containing the Pb cations with empty 6s states and the oxidation number exceeding 2. However, we find that no XANES spectrum of the Pb L_3-edge of Pb-modified

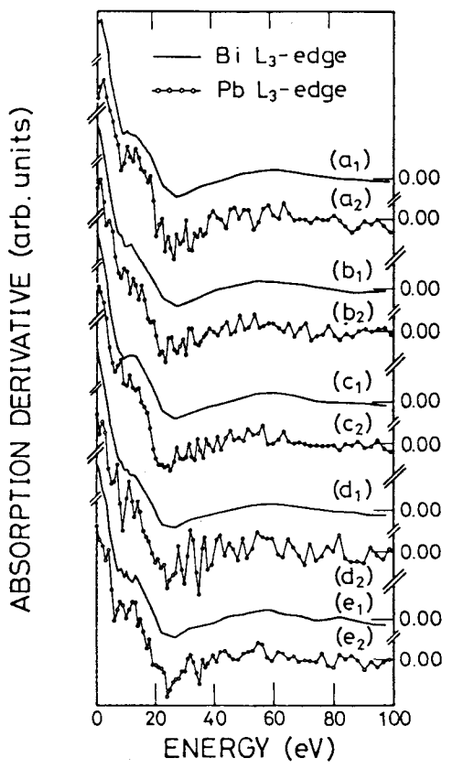

FIG. 6(b). Derivatives of the spectra of the Bi L_3-edge for the 2223 sample (a_1), the 2201 samples with T_c = 13 K (b_1) and non-superconductive (c_1), and the Pb-BSCCO samples with x = 0.2 (d_1) and 0.4 (e_1) and derivatives of the spectra of the Pb L_3-edge for the 2223 sample (a_2), the 2201 samples with T_c = 13 K (b_2) and non-superconductive (c_2), and the Pb-BSCCO samples with x = 0.2 (d_2) and 0.4 (e_2).

samples exhibits such a bump, expected to be located near -6 eV, corresponding to the allowed dipole transition from the $2p^{3/2}$ states to unoccupied 6s states. The channel from $2p^{3/2}$ to the states with s symmetry is generally much weaker than the channel from $2p^{3/2}$ to the states with d symmetry. The XANES spectrum of the Pb L_3-edge of Pb_3O_4, in which the oxidation number of some Pb cations is 4, also exhibits no bump corresponding to the transitions from 2p to 6s. (Although the low-lying bump is easily observed in the derivative of XANES of the Pb L_3-edge of Pb_3O_4, the signal-to-noise ratio of the XANES spectra of Pb L_3-edge of the samples, containing small concentration of Pb, is too small to allow us to take the derivatives of the XANES spectra of the samples to discover the low-lying bump from the derivatives of the XANES

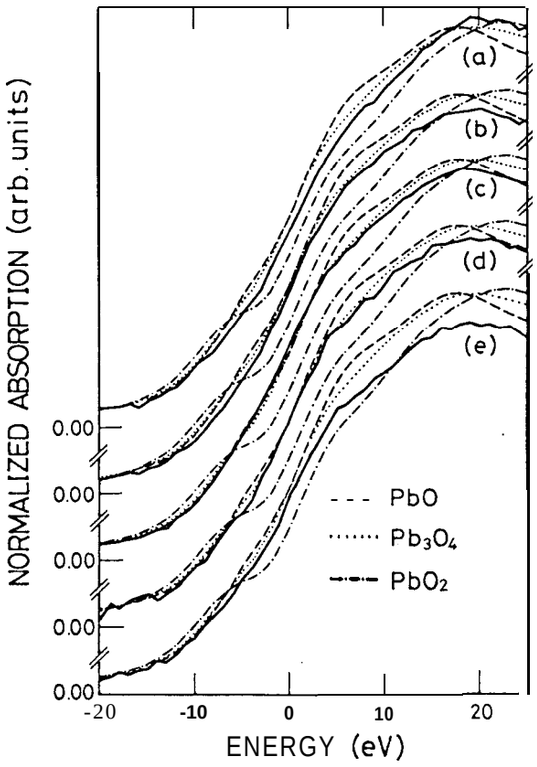

FIG. 7. X-ray-absorption near-edge structures in the vicinity of the Pb L_3-edge for the 2223 sample (a), the 2201 samples with T_c = 13 K (b) and non-superconductive (c), and the Pb-BSCCO samples in which x = 0.2 (d) and 0.4 (e). The curves superimposed over each curve of the data of these samples present the X-ray absorption near-edge structures of the Pb L_3-edge of PbO, PbO_2, Pb_3O_4 for comparison. The curves have been shifted vertically for clarity and the the energy zero refers to 13035 eV.

spectra.) Besides, for the Pb L_3-edge of the Pb-modified samples there are no significant shifts toward higher energy compared with those of PbO and Pb_3O_4, whereas the aspects of the XANES spectra of the Pb Lx-edge of the samples are similar to those of the spectrum of Pb_3O_4. Hence, the oxidation number of the total substituted Pb in the Pb-modified samples cannot be 4 but the existence of some Pb with oxidation number exceeding 2 cannot be precluded.

III-3. Cu K-edge

The orientation-dependent near-edge structures measured in the vicinity of the Cu K-edge for the aligned 2223 sample and for an unpolarized CuO sample and their derivatives are illustrated in Fig. 8 and 9 respectively. Although there have been published several interpreta-

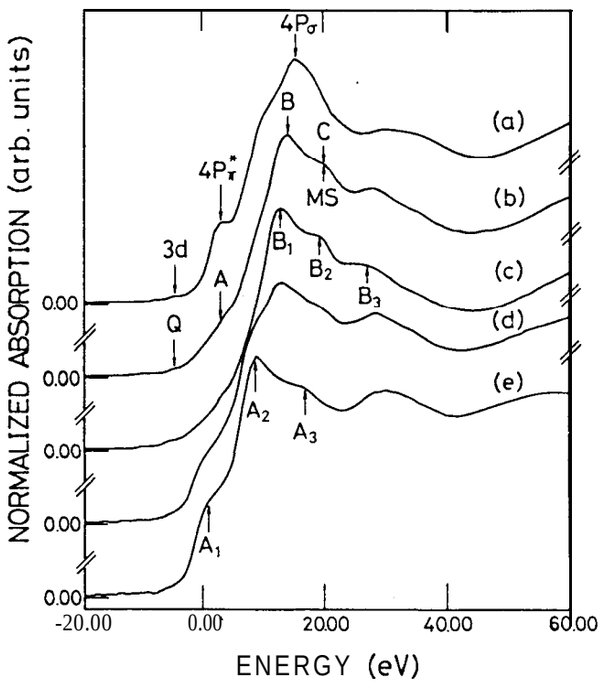

FIG. 8. Unpolarized XANES spectra of the Cu K-edge for CuO (a) and for the 2223 sample (b) alongwith polarized $\mathbf{E}\perp\mathbf{C}$ (c), $\angle EC < 45°$ (d) and $\mathbf{E}\|C$ (e) XANES spectra of the Cu K-edge for the 2223 sample. The curves have been shifted vertically for clarity and the energy zero refers to the K-absorption edge (8980 eV) of pure Cu.

tions[33-35] of the features of Cu K-edge XANES spectra, it was premature to separate readily and to identify definitely the features of the XANES of the Cu K-edge without both sophisticated calculations and improved experimental data. In preliminary works the commonly accepted interpretations of the features,[36,20] in particular of the peaks A and C in curve (b) in Fig. 8, are assigned as follows. (1) The small pre-edge feature Q indicates the ls-to-3d quadrupole transition. (2) The set of features falling between the labels A and B is dominated by an overlap of the dipole-allowed direct transitions to Cu 4p-like final states which are split into out-of-plane ($4p\pi$) and in-plane ($4p\sigma$) states by crystal-field effects. The shoulder at $4p\pi^*$, clearly observed in the curve of XANES for CuO and corresponding to A in the curve of XANES of the 2223 sample, is attributed to transitions to the $4p\pi^*$ state. The asterisk indicates that the 1s-to-$4p\pi$ transition accompanied by a shake-down transition associated with charge transfer from the ligand to the metal; this charge transfer enhances the screening of the core hole and decreases the transition energy from that associated with p states. The main peak B at the top of the edge

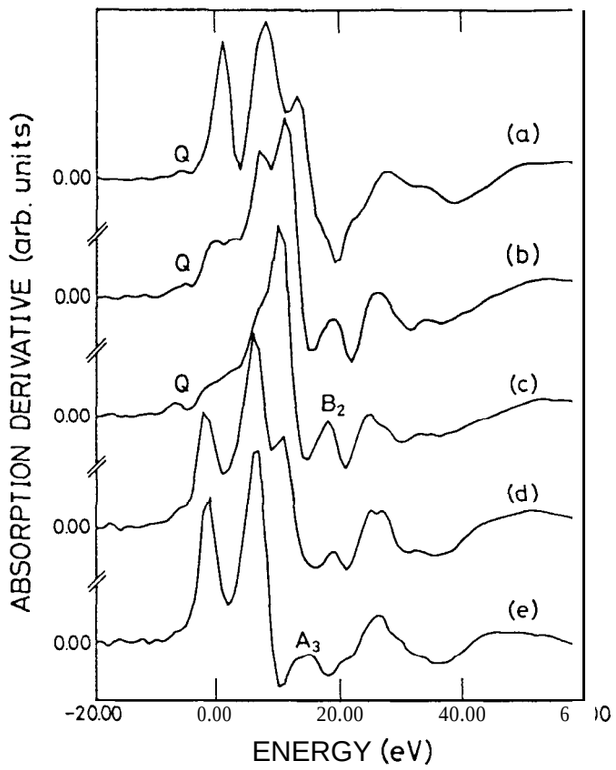

FIG. 9. Derivative of the spectra in Fig. S for CuO (a) and for the 2223 samples of which the c axis is random (b), parallel to E (e) and vertical with respect to E (c).

is attributed to the transition to $4p\sigma$ states. (3) The edge feature C, which is the signature of EXAFS multiple scattering (MS) within the Cu-0 plane, is associated with the signature of EXAFS contributions from high-shell neighbors.

Recent work has included the application of the multiple-scattering approach in real space for XANES spectra of the Cu K-edge,[37,38] simple Hartree-Fock cluster calculations,[39] and experimental studies of related superconducting compounds-particularly the orientation-dependent measurements!' By these means we understand the nature of absorption processes[41,37] more clearly than before and wc are thus able to reinterpret the features of XANES spectra of the Cu K-edge.

In the process of X-ray absorption, a photoelectron moves outward and a core hole is created suddenly by the incident X-ray. The system may undergo a complicated relaxation processes, which are the so-called many-body effects induced by the excited photoelectron-hole dipole and which *arc* certainly important *and* even dominant in the threshold region in XAFS,

including shake-up or shake-down. In the high T_c copper oxide superconductor, both 0 2p holes and Cu 3d holes are present. These holes, which are initially shared between the Cu and 0 atoms, interact strongly with the core-hole or the slow photoelectron present in the final state, either moving almost onto the oxygens to form a well-screened Cu $3d^{10}\underline{L}$ configuration (for which $\underline{L}$ indicates a hole on the ligand oxygens) or shifting almost completely onto Cu to yield a poorly screened Cu $3d^9$ configuration. Therefore, the many-body relaxation, subject to conflicting interpretation, results in a change of the admixture of the electron configurations in the final states. The admixture of the valence configurations of Cu, determined by the polarized XANES, has been influenced by many-body effects and cannot reveal directly the inherent electron configuration of Cu before the interaction with the incident X-ray.

After a careful analysis in terms of one-electron transitions, which are calculated on the basis of the various electronic configurations of the absorbing Cu atom resulting from many-body effects, one can identify the presence of specific many-electron features in polarized XANES spectra. As illustrated in curves (c) and (e) in Fig. 8, for X-ray radiation polarized along the crystal c axis and in the ab plane, the satellites A3 and B_2 are assigned to the poorly screened core hole with $3d^9$ electronic configuration of the central Cu ion, *i.e.,* to $\underline{1s}\,3d^9,\varepsilon p^1$ final state, whereas the main peaks A_2 and B_1 are assigned to the fully relaxed and well screened core hole with Cu $3d^{10}\underline{L}$ electronic configuration, *i.e.,* to the final state configuration $\underline{1s}3d^{10}\varepsilon p^1$. Here, εp means the p-like (I = 1) states projected on the Cu site with orbital angular momentum $m_1 = 0$ in the E || C spectra, and the $m_1 = 1$ for the $\mathbf{E}\perp\mathbf{C}$ spectra and the underline denotes a hole in corresponding state. The peaks A_1 and A_2 are assigned as the transitions, determined by resonance of the mutiple scattering pathways involving mainly Ca, Sr, O(apex) together within Ca and SrO layers in real space, to states delocalized over a large cluster of atoms. The peaks A_1 and A_2 appearing in the E || C polarized spectrum are proportional to the *partial* density of unoccupied states, whereas the variation of the relative heights of the peaks A_1 and A_2 does *not* reveal the influence of many-body effects. The peaks B_1 and B_3 of $\mathbf{E}\perp\mathbf{C}$ polarized XANES for the 2223 sample are due to the transitions, given by resonance of the multiple scattering of the photoelectron by O(plane) and Cu ions in the four neighboring Cu sites in the Cu-0 plane, to the final states delocalized over a large cluster of atoms.

The peak B_2 in rhe $\mathbf{E}\perp\mathbf{C}$ polarized spectra of the Cu K-edge, which was previously assigned only to EXAFS multiple scattering within the Cu-0 plane in copper-oxide superconductor, is assigned to a many-body peak. The peak A3 in the E || C polarized spectra is also attributed to a many-body peak. Several conflicting hypotheses concerning the peaks A3 and B_2 deserve attention. Li et al.[40] proposed that the intense multielectron-excitation satellites about 7 eV from the main peak in XANES of the Cu K-edge seem characteristic of a largely non-isotropic Cu site. Guo et al.[42] suggested that these multielectron excitation features involve the dipole-allowed relaxation channels for the Cu 3d → 4p transition in the sample with certain symmetry of the copper sites for X-ray radiation polarized along the crystal c axis and in the ab plane. Tolen-

tino et al.[41] advocated the need to take into account the role of the slow photoelectron in the many-body relaxation which leads to electron transfer from O 2p to fill a hole in Cu 3d in cuprates.

Bianconi et al. found no obvious A3 peak in the polarized XANES spectrum of the Cu K-edge measured for $Bi_2CaSr_2Cu_2O_8$.[37] In contrast, we observe clearly the peak A3 in the E||C spectra, according to the polarized XANES curve in Fig. 8 measured for the 2223 sample. The peak A3 is also observed from the derivative of the E||C polarized XANES spectrum shown in Fig. 9. If the feature A_1 appearing in the E||C spectrum is indeed due to the shake-down effect, then in the **E⊥C** spectrum a similar shake-down peak on the rising edge may also be present. In the **E⊥C** polarized XANES spectra of the Cu K-edge of the 2223 sample no identification of such a peak, which one expects to be located on the rising pre-edge according to this interpretation, is observed. The derivatives of the *polarized* XANES spectra of the Cu K-edge of the 2223 sample (cf. curves (c) and (e) in Fig. 9) clearly reveal that the bump, which corresponds to the 3d quadrupole transition located at about -6 eV, appears in the derivative of only the **E⊥C** polarized XANES spectra of the Cu K-edge for the 2223 samples, because only in the condition **E⊥C** the quadrupole transition to the empty $3d_{x^2-y^2}$ orbitals is allowed. This result is consistent with the well established conclusion, based on the XANES data of the Cu L_3-edge,[28] that most holes at the Cu site are located in $3d_{x^2-y^2}$ orbitals oriented parallel to the Cu-O plane.

In Fig. 10 the XANES spectra of the 2201, 2212 and 2223 samples are illustrated. The intensity of A_1 is enhanced going from the 2223 sample with two Ca layers, the 2212 sample with one Ca layer to the 2201 samples without Ca layer and indeed depends strongly on the Ca and SrO layers. The intensities of the peaks C of the XANES spectra of the Cu K-edge for the 2223 sample and for the 2201 sample without superconductivity are extremely different from each other. Fig. 11 shows the magnitudes of the Fourier transforms of $k^3\chi(k)$ of the two samples. The first peak located at ~ 1.5 A, appearing in each plot of the magnitudes of the Fourier-transforms, is predominantly due to the four O nearest neighbours within the Cu-O plane. The peak located at ~ 2.7 Å corresponds to the Ca and Sr atoms around the Cu absorbing atom. The third peak (Cu-Cu peak) located at ~ 3.6 A, appearing in each curve of the magnitudes of the Fourier-transforms, has a great amplitude because of focused multiple scattering via intervening oxygen atoms.[43] The appearance of the focusing effect indicates that the Cu-O planes within the samples have an ordered planar structure, viz., not only is the distance between each Cu atom and the nearest Cu atoms almost equivalent, but also the positions of the Cu atoms and the intervening oxygen are nearly collinear. Although the ordered structure of the Cu-O planes has been confirmed by the XAFS data, we find the Cu-Cu peak in the curve of the magnitude of $k^3\chi(k)$ for the 2223 sample is broader and lower relative to that in the curve of the magnitude of $k^3\chi(k)$ for the 2201 sample without superconductivity (Fig. 11). This discrepancy of the line shapes indicates that in the 2223 sample there is more significant distortion of the internuclear Cu-Cu line via the intervening oxygen atom or, more likely, a more significant displacements of

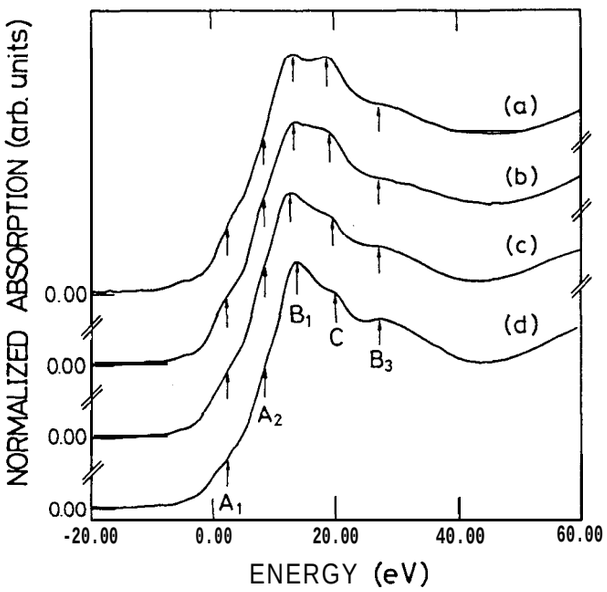

FIG. 10. X-ray-absorption near-edge spectra, measured at the Cu K-edge and normalized to the edge step, for the non-superconductive 2201 sample (a), the 2201 sample with T_c = 13 K (b), the 2212 sample (c) and the 2223 sample (d). The energy zero corresponds to 8980 eV.

the Cu atoms from their average position. A *partial* contribution of the feature B_2 is reproduced in the mutiple-scattering calculation by taking into account larger cluster of at least eight shells, whereas the features B_1 and B_3 are reproduced in the mutiple-scattering calculation by considering smaller cluster of lesser shells. For this reason the features B_1 and B_3 seem less sensitive to the faint variation of the Cu-0 planar structure; hence the position and relative height of the peaks B_1 and B_3 in the XANES spectra of the 2223 sample are roughly similar to those of the peaks B_1 and B_3 in the XANES spectra of the 2201 sample with non-superconductivity. In contrast, *the C satellite, which consists of superposition predominantly of B_2 and partially of A_3*, moves slightly toward lower energy and its intensity obviously increases going from the 2223 sample to the 2201 sample without superconductivity. Following Bianconi et al.,[37] we believe that the increase of the intensity of C in the unpolarized spectra reflects mainly the increase of that of *peaks B_2, due partially to the many-body effects and partially to the resonance of the multiple-scattering pathways mainly involving the Cu and 0 atoms in the Cu-O plane.* This result is consistent with the result reported by Bianconi et al.[37] who observed the intensity of the peak B_2 of the XANES spectra of the insulating $Bi_2Sr_2YCu_2O_{8+\delta}$ phase to increase relative to the superconducting $Bi_2Sr_2CaCu_2O_{8+\delta}$ phase at room temperature. However, it is difficult to determine whether the predominant factor, which causes the variations of peaks C of the samples, is the many-body

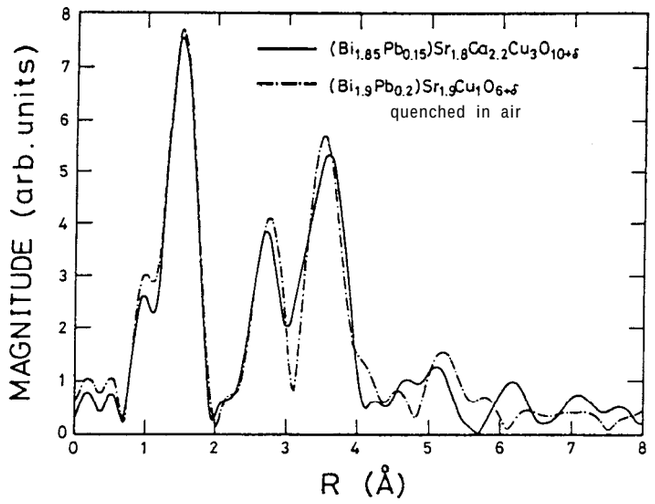

FIG. 11. Magnitudes of the Fourier-transforms of k%(k) over the k-range 2.79-11.14 $Å^{-1}$ converted by choosing E_0 at the half-height point of the Cu K-edge for the 2223 sample and the non-superconductive 2201 sample.

effects possibly relating to the change of the isotropy of the structure around the Cu site or the multiple-scattering resonance being sensitive to the distortion of the Cu-0 plane. Nevertheless, we believe the observable variations-particularly the variation of the Cu-Cu peak-of the magnitude of the Fourier transform of $\chi(k)$ of the corresponding sample cannot be ignored in clarifying the origin of the variations of peaks C in the unpolarized XANES spectra *(i.e.* peaks B_2 in the $\mathbf{E} \perp \mathbf{C}$ polarized XANES spectra) of the 2223, 2212, 2201 (T, = 13 K, non superconductive) samples. The detailed description of the many-body final states A3 and B_2 is beyond the scope of our work and is not yet carried out although several conflicting hypotheses conducting the nature of the many-body effects have been proposed.

IV. CONCLUSIONS

Prudently using the XAFS technique and taking into account its restrictions, we have extracted information about the properties of the Bi-0 layers and the substituted Pb atoms in the Bi-Sr-Ca-Cu-0 system. We have deduced the ordered structure of the Cu-0 planes which are responsible for the superconductivity of the copper-oxide high T_c superconductors.

Specifically, in all families of the Bi-Sr-Ca-Cu-0 system the modulation structures in the Bi-0 layers are present. Because of the symmetry of the coordination geometry of the nearest oxygen atoms around the Bi cation, it seems less reliable to extract related structural and

electronic information about the Bi cation by means of polarized XAFS data for these Bi-Sr-Ca-Cu-0 superconductors. Despite the oxidation number of some Bi cations being 3, that of the remaining Bi cations exceeds 3. The XAFS data provides the necessary evidence, which reveals that the lead atoms in the added lead oxide substitute for some Bi atoms in the Bi-0 layers of the Bi-Sr-Ca-Cu-0 system. The oxidation number of all substituted Pb cation in the Bi site cannot be 4, and the oxidation number of a fraction of the substituted Pb cations is 2.

We have found peak A3 in the polarized E || C spectrum of the Cu K-edge for the 2223 sample. We have noticed the variation of the features A_1 and B_2 (A_3) going from the 2223 samples to 2201 samples. The main open problem concerns the detailed nature of the many-body effects involving manifold relaxation channels. Consequently, further experimental and theoretical work is needed to determine how the admixture of the inherent electronic configurations of Cu within the Bi-Sr-Ca-Cu-0 system combined with the many-body effects affect the change of the admixture of the electronic configuration of the absorbing atom after the excitation of incident X-ray. The change results in the variation of the relative positions and particularly of the relative intensities of the main peaks and corresponding satellites in XANES of the Cu K-edge.

ACKNOWLEDGMENTS

We are grateful to Dr. Chau-Ting Chang for his gracious help. We also express our appreciation to Prof. P. K. Tseng and Dr. B. A. Bunker for their help to obtain the beam time. This work was supported by the National Science Council of the Republic of China under grant No. NSC 81-0208-M-032-13 to W. F. Pong.

REFERENCES

1. S. Uchida, H. Takagi, K. Kitazawa, and S. Tanaka, Jpn. J. Appl. Phys. 26, L1 (1987).
2. M. K. Wu, J. R. Ashburn, C. J. Torng, P. H. Hor, R. L. Meng, L. Gao, Z. J. Huang, Y. Q. Wang, and C. W. Chu, Phys. Rev. Lett. 58,908 (1987).
3. H. Maeda, Y. Tanaka, M. Fukutomi, and T. Asano, Jpn. J. Appl. Phys. 27, L209 (1988).
4. C. Michel, M. Hervien, H. M. Borel, A. Grandin, F. Deslandes, J. Provost, and B. Raveau, Z. Phys. B68, 421 (1987):
5. J. Akimitsu, A. Yamazaki, H. Sawa, and H. Fujiki, Jpn. J. Appl. Phys. 26, L2080 (1987).
6. M. Takano, J. Takada, K. Oda, H. Kitaguchi, Y. Miura, Y. Ikeda, Y. Tomii, and H. Mazaki, Jpn. J. Appl. Phys. 27, L1041 (1988).
7. M. Mizuno, H. Endo, J. Tsuchiya, N. Kijima, A. Sumiyama, and Y. Oguri, Jpn. J. Appl. Phys. 27, L1225 (1988).
8. A. Sequeira and J. V. Yakhmi, Phys. Rev. B45, 2527 (1992).
9. C. S. Gopinath and S. Subramanian, Phys. Rev. B45, 7513 (1992).

10. H. Nobumasa, T. Arima, K. Shimizu, Y. Otsuka, Y. Murata, and T. Kawai, Jpn. J. Appl. Phys. 28, L57 (1989).
11. N. Kijima, H. Endo, J. Tshuchiya, A. Sumiyama, M. Mizuno, and Y. Oguri, Jpn. J. Appl, Phys. 28, L787 (1989).
12. L. Pierre, J. Schneck, D. Morin, J. C. Toledano, J. Primot, C. Daguet, and H. Savary, Ferroelectrics **105**, 81 (1990).
13. A. Sequeira, J. V. Yakhmi, R. M. Iyer, H. Rajagopal, and P. V. P. S. S. Sastry, Physica C 169, 291 (1990).
14. S. X. DOU, H. K. Liu, A. J. Bourdillon, M. Kviz, N. X. Tan, and C. C. Sorrell, Phys. Rev. B40, 5266 (1989).
15. B. 0. Wells, X.-X. Shen, D. S. Dessau, W. E. Spicer, C. G. Olson, D. B. Mitzi, A. Kapitulnik, R. S. List, and A. Arko, Phys. Rev. Lett. **65**, 3056 (1990).
16. For general references to XAFS the following review article is helpful: D. C. Koningsberger, R. Prins, Principles, Application, Techniques of EXAFS, SEXAFS and XANES, John Wiley & Sons, Inc., New York (1987).
17. N. H. Wang, C. M. Wang, H. C. I. Kao, D. C. Ling, H. C. Ku, and K. H. Lii, Jpn. J. Appl. Phys. 28, L1505 (1989).
18. A. Maeda, M. Hase, I. Tsukada, K. Noda, S. Takebagashi, and K. Uchinokura, Phys. Rev. B41, 6418 (1990).
19. J. B. Shi, B. S. Chiou, and H. C. Ku, Phys. Rev. **B43**, 13001 (1991).
20. C. H. Chou, W. F. Pong, I. N. Lin, and S. F. Tsai, Chin. J. Phys. 29,263 (1991).
21. D. E. Farrell and B. S. Chandrasekhar, Phys. Rev. **B36**, 4025 (1987).
22. Ref. 16, pp. 216.
23. G. Malmros, Acta. Chem. Scand. 24,384 (1970).
24. Y. Matsui, S. Takekawa, H. Nozaki, A. Umezono, E. Takayama-Muromachi, and S. Horiuchi, Jpn. J. Appl. Phys. 27, L1241 (1988).
25. C. H. Chen, D. J. Werder, S. H. Liou, H. S. Chen, and M. Hong, Phys. Rev. **B37**, 9834 (1988) and references therein.
26. J. Schneck, L. Pierre, J. C. Toledano, and C. Daguet, Phys. Rev. **B39**, 9624 (1989).
27. J. G. Wen, C. Y. Yang, Y. F. Yan, and K. K. Fung, Phys. Rev. **B42**, 4117 (1990).
28. A. Bianconi, S. D. Longa, C. Li, M. Pompa, A. Congiu-Castellano, D. Udron, A. M. Flank, and P. Lagarde, Phys. Rev. **B44**, 10126 (1991).
29. J. Stöhr and R. Jaeger, Phys. Rev. **B27**, 5146 (1983).
30. S. Salem-Sugui, Jr., E. E. Alp, S. M. Mini, M. Ramanathan, J. C. Campuzano, G. Jennings, M. Fuiz, S. Pei, B. Dabrowski, Y. Zheng, D. R. Richards, and D. G. Hinks, Phys. Rev. **B43**, 5511 (1991). S. M. Heald and D. Dimarzio, M. Crof and M. S. Hegde, S. Li, and M. Greenblatt, Phys. Rev. **B40**, 8828 (1989).
31. J. C. Bailar, H. J. Emeleus, S. R. Nyholm, and A. F. Tortman-Dickenson, COMPREHENSIVE

INORGANIC CHEMISTRY, Vol. 2, Pergamon Press Ltd., Oxford (1973).
32. J. B. Boyce, F. G. Bridges, T. Claeson, T. H. Geballe, and J. M. Remeika, Phys. Rev. **B41**, 6306 (1990).
33. D. DiMarzio, H. Wiesmann, D. H. Chen, and S. M. Heald, Phys. Rev. **B42**, 294 (1990).
34. N. Kosugi, Y. Tokura, H. Takagi, and S. Uchida, Phys. Rev. **B41**, 131 (1990).
35. Z. Tan, J. I. Budnick, C. E. Bouldin, J. C. Woicik, S.-W. Cheong, A. S. Cooper, and G. P. Espinosa, Phys. Rev. **B42**, 1037 (1990).
36. C. Y. Yang, A. R. Moodenbaugh, Y. L. Wang, Youwen Xu, S. M. Heald, D. 0. Welch, M. Suenaga, D. A. Fischer, and J. E. Penner-Hahn, Phys. Rev. **B42**, 2231 (1990).
37. A. Bianconi, C. Li, F. Campanella, S. D. Longa, I. Pettiti, M. Pompa, S. Turtu, and D. Udron, Phys. Rev. **B44**, 4560 (1991).
38. A. Bianconi, C. Li, S. D. Longa, and M. Pompa, Phys. Rev. **B45**, 4989 (1992).
39. J. M, Tranquada, S. M. Heald, W. Kunnmann, A. R. Moodenbaugh, S. L. Qiu, Y. Xu, and P. K. Davies, Phys. Rev. **B44**, 5176 (1991).
40. C. Li, M. Pompa, A. C. Castellano, S. D. Longa, and A. Bianconi, Physica C 175,369 (1991).
41. H. Tolentino, M. Medarde, A. Fontaine, F. Baudelet, E. Dartyge, D. Guay, and G. Toruillon, Phys. Rev. **B45**, 8091 (1992).
42. J. Gao, D. E. Ellis, G. L. Goodman, E. E. Alp, L. Soderholm, and G. K. Shenoy, Phys. Rev. B41, 82 (1990).
43. P. P. Lottici, G. Antonioli, and F. Licci, Physica. **C152**, 468 (1988).